

Synthesis, Characterization, and Processing of Highly Bioadhesive Polyurethane Urea as a Microfibrous Scaffold Inspired by Mussels

Giovanni Carlo Miceli, Annalisa Martorana, Francesco Cancilla, Giovanna Pitarresi, Mariano Licciardi, and Fabio Salvatore Palumbo*



Cite This: *ACS Appl. Polym. Mater.* 2023, 5, 8483–8494



Read Online

ACCESS |



Metrics & More



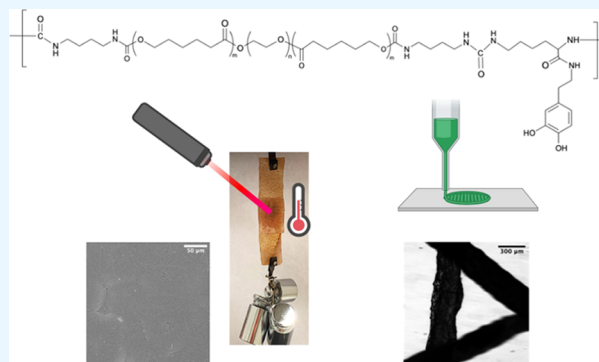
Article Recommendations



Supporting Information

ABSTRACT: The need to obtain solid adhesive scaffolds that can be processed to create friendly microenvironments, direct cellular behaviors, and tissue regeneration is growing. A facile method was used to incorporate a mussel-inspired adhesive moiety, dopamine, into segmented polyurethanes based on polycaprolactone–polyethylene glycol–polycaprolactone (PCL–PEG–PCL) copolymers. Dopamine was chemically bonded to lysine and used as a chain extender to obtain a solid biodegradable elastomer capable of strongly adhering to different materials after melting occurs. Lysine alone was used as a chain extender to produce a similar polyurethane control group. The low melting point (55 °C) opens multiple possible applications for this polyurethane. A complete chemical–physical characterization was performed, and adhesion strength was evaluated in a lap shear configuration. The interaction with a high-energy surface like glass and aluminum at room temperature was remarkable (respectively 2.8 and 2.6 MPa). The adhesion was also evaluated with porcine skin underwater at 37 °C, resulting in 30 kPa. Over a period of 6 months, the material undergoes slow hydrolytic degradation. Nevertheless, the material and its degradation products were not cytotoxic. The polymer was then processed with melt extrusion three-dimensional (3D) printing to obtain oriented microfibers, producing different scaffolds.

KEYWORDS: bioadhesives, mussel inspired, polyurethanes, biomaterials, melt extrusion



1. INTRODUCTION

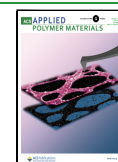
Adhesion is a physicochemical phenomenon of attraction between dissimilar molecular species. It is caused by molecular interactions at the interface between materials but also depends on surface properties and environmental conditions.¹ For instance, high-energy surfaces favor adhesion, while high temperatures reduce it. Furthermore, spreading adhesives is essential to allow the best distribution of stresses between the bonded joints. When at least one of these joints is a biological component (i.e., tissue, organ, or cell), the adhesive is known as a bioadhesive.² Cyanoacrylate-based, characterized by high bonding strength and short gluing time, were the first used bioadhesives and are currently used in plastic surgery, skin transplantation, and emergency wound treatment.^{3,4} Yet, these products are limited to topical conditions due to their toxic degradation products.⁵ Glutaraldehyde-based bioadhesives possess strong wet bonding strength and have been widely used in Europe and Japan for treating aortic dissections and in diverse surgical operations. Nevertheless, the formaldehyde molecule carries mutagenicity and carcinogenicity.^{6,7} Compared to glutaraldehyde-based bioadhesives, the cytotoxicity of dextran–polylysine is 1000 lower while maintaining a remarkable adhesion strength.⁸

In adhesion technology, it is well known that water is the main reason for adhesive failure.⁹ Indeed, there are several ways in which it can compromise the performance of the adhesive, like interfacial wicking and crazing, or it can induce swelling and hydrolysis.¹⁰ However, nature is a source of inspiration by providing many outstanding examples of adhesive strategies. In fact, the challenges of developing tough and robust underwater bonding are analogous to the adhesion problems solved by many marine organisms, which have developed adhesive strategies to deal with the dynamic sea environment.¹¹ Marine mussels are naturally equipped with reliable strategies to achieve interfacial adhesion at the tidal interface in dynamic and turbulent environments. Mussels are bivalve molluscs, and their feet enable them to attach by byssus threads to a solid substrate. The byssus is a bundle of radially distributed threads that terminate in an adhesive plaque

Received: July 14, 2023

Accepted: September 5, 2023

Published: September 18, 2023



attached to rocks, preventing them from being dislodged and crushed by turbulence and waves. They attach to inanimate and living surfaces in both freshwater and marine environments by secreting adhesive proteins that harden in situ. These proteins, isolated from mussel byssus, have been shown to bond with numerous substrates, including glass, Teflon, wood, concrete, plastics, metals, biological cell lines, bone, teeth, and others.^{1,12–15} Nevertheless, these outstanding adhesive systems that allow them to affix themselves over wide ranges of temperature, salinities, and movements are not yet well mimicked by human technologies. Therefore, the exploration of biomaterials that are capable of strongly but safely interacting with tissues is never-ending. Indeed, scientists have performed detailed studies of the chemistry behind the complex adhesion mechanisms of mussels as a potential source for a water-resistant bioadhesive, opening a wide range of possible applications.¹⁶ Surgical glues could ensure faster wound closure than conventional stitching methods and avoid the damage caused by sutures. Mehdizadeh et al. prepared injectable biodegradable adhesives that promote wound healing while avoiding inflammation.¹⁷

Bioadhesive drug delivery systems could reach different body regions to locally release drugs over extended periods. Xu et al. used a sulfasalazine-loaded catechol-modified chitosan hydrogel as an injectable mucoadhesive formulation to treat ulcerative colitis.¹⁸

Indeed, inorganic implantable materials have been widely used in various biomedical applications, such as metallic endoprosthesis, bioactive glasses or ceramics, sensors, or devices for nerve stimulation.^{19,20} However, the integration of these materials with biological tissues often presents challenges related to poor adhesion and sealing at the interface, mechanical mismatch, and an inflammatory tissue response that can lead to scar tissue encapsulation of the implant and subsequent device failure.

Bioadhesive coatings play a crucial role in improving the performance and functionality of inorganic implantable materials by promoting tissue adhesion, reducing implant-related complications, and improving long-term biocompatibility. These coatings act as a bridge between the implant surface and the surrounding biological environment, promoting tissue integration, reducing inflammation and infection rates, and improving the long-term stability of implants. The biomedical applications of these bioadhesive coatings span from orthopedic implants, to promote osteointegration and improve implant stability, to cardiovascular stents, neural implants, and tissue engineering scaffolds, which improve biointegration and reduce complications such as mechanical mismatch, thrombosis, and implant migration.

In the tissue engineering field, mussel-inspired bioadhesives could guarantee tissue adhesion while carrying biomolecules to induce cell growth.¹⁵ However, glues do not have suitable physical properties to be processed as biomaterials with controlled shapes and architectures. The synthesis of a bioadhesive polymer that can be processed with specific manufacturing techniques as a solid biomaterial could increase the current biomedical applications of tissue adhesive biomaterials. Here, a bioadhesive polyurethane urea derivative was first synthesized by using PCL–PEG–PCL as a block copolymer having a nominal ratio of PCL/PEG equal to 30 and lysine–dopamine (LDA) as an extender derivative. When melted at a temperature of 55 °C and then cooled, the lysine–dopamine-containing polyurethane urea (PU-LDA) films

exhibit robust adhesive properties on high-energy surfaces such as aluminum, glass, and even porcine skin. A rheological study of melted PU-LDA was performed to evaluate its potential suitability for melt extrusion three-dimensional (3D) printing. Therefore, we produced different microfiber patterns by using this adhesive polymer.

2. MATERIALS AND METHODS

2.1. Materials. Dopamine hydrochloride (DA-HCl), di-*tert*-butyl dicarbonate [(Boc)₂O], sodium bicarbonate (NaHCO₃), 1-ethyl-3-(3-dimethyl aminopropyl)carbodiimide hydrochloride (EDC-HCl), triethylamine (TEA), dimethylformamide DMF-*d*₇, chloroform-*d*, dimethyl sulfoxide DMSO-*d*₆, polyethylene glycol 1000 Da (PEG), ϵ -caprolactone (ϵ -CL), lithium bromide (LiBr), diethylamine (DEA), standards of PEG, sodium azide (NaN₃), Dulbecco's phosphate buffered saline (DPBS), L-lysine hydrochloride, *N*-hydroxysuccinimide (NHS), tetrahydrofuran (THF), and ethyl acetate (EA) were purchased from Merck (Germany).

Calcium hydride (CaH₂), stannous octoate [Sn(Oct)₂], and 1,4-diisocyanatobutane (BDI) were purchased from Fluka (Italy) and used without further purification.

Dimethyl-formamide (DMF), diethyl ether, dichloromethane (DCM), toluene, methanol, 2-propanol, and acetone were purchased from VWR (Italy) and used without further purification.

Dulbecco's modified Eagle's medium (DMEM), fetal bovine serum (FBS), trypsin, L-glutamine, penicillin, streptomycin, and amphotericin were purchased from Euroclone Group (Italy).

2.2. Apparatus. Hydrogen nuclear magnetic resonance (¹H NMR) spectra were recorded using a Bruker Avance II 300 MHz instrument at room temperature in DMSO-*d*₆ for LDA, DMF-*d*₇ polyurethane urea (PUUs), and chloroform-*d* for PCL–PEG–PCL.

Fourier transform infrared spectroscopy analysis in total attenuated reflectance (ATR-FTIR) was performed using a Bruker Alpha instrument in a wavenumber range of 400 to 4000 cm^{−1} at room temperature on KBr tablets.

Ultraviolet (UV) measurements were performed by using a spectrophotometer. UV–visible spectra were recorded with a Shimadzu UV-2400 spectrophotometer.

The analysis of size exclusion chromatography (SEC) was conducted with an Agilent 1260 Infinity multidetector GPC/SEC system. The elution was performed on a Phenogel 5 μ m with a 10³ Å pore size column using LiBr/DMF 0.025 M as a mobile phase at 50 °C with a flow rate of 0.8 mL/min. Standards of PEG were used for calibration.

Differential scanning calorimetry (DSC) measurements were performed using a DSC 131 EVO, SETARAM Instrument. Samples were weighed and hermetically sealed in aluminum pans and heated from −50 to 150 °C with a heating rate equal to 5 °C/min to measure melting (*T*_m) and glass (*T*_g) transition temperatures.

The hydrophilicity was studied by a video contact angle instrument in the FTA 1000 C class, First Ten Angstroms.

Rheological experiments were carried out using a DHR-2 oscillatory rheometer TA Instruments equipped with a self-heating Peltier plate. The geometry used for all tests was a parallel flat plate device with a diameter of 20 mm.

The heat required to generate spot melting on the PU-LDA films was produced by irradiating with a GBox diode near-infrared (NIR) laser (λ = 810 nm).

Adhesive testing was performed by tensile measurements in a lap shear configuration using a Bose TA Instruments ElectroForce Test Bench System.

The microfibrinous scaffold was produced by 3D printing using a BioAssemblyBot 400.

Scanning electron microscopy (SEM) images were acquired with a Phenom PRO X instrument.

2.3. Synthesis of PU-LDA and Chemical–Physical Characterization. The triblock copolymer PCL–PEG–PCL was synthesized by ring-opening polymerization (ROP), setting a molar ratio between ϵ -CL and PEG equal to 30.²¹

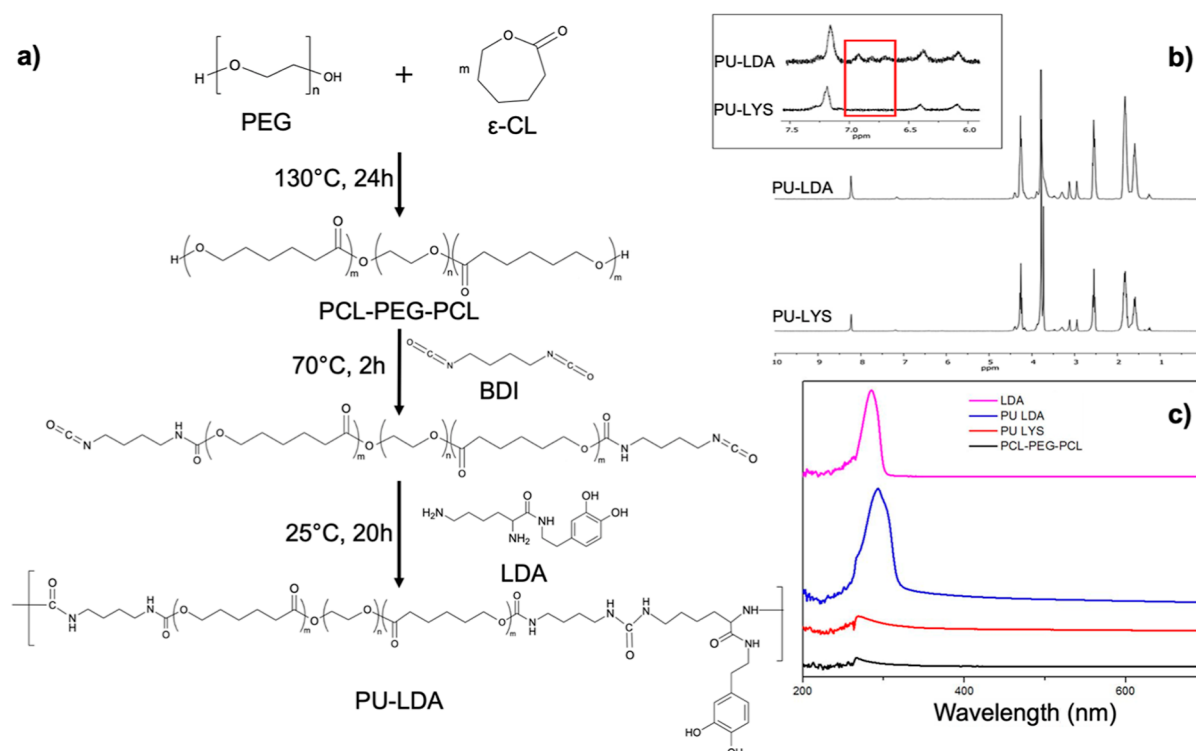


Figure 1. (a) Scheme of PU-LDA synthesis, (b) ^1H NMR comparison between PU-LDA and PU-LYS, and (c) UV-vis comparison between synthesized products.

Before the reaction, ϵ -CL was distilled at 65 °C with calcium hydride (CaH_2) under vacuum, and PEG was dehydrated by azeotropic distillation in toluene at 76 °C and room pressure.

The copolymer synthesis was carried out at 130 °C for 24 h with $\text{Sn}(\text{Oct})_2$ as the catalyst in an argon atmosphere. Then the product was purified by dropwise precipitation in cold diethyl ether under stirring, then washed in 2-propanol, and kept at 4 °C overnight. Finally, the product was dried under vacuum, resulting in a white powder. Copolymer was characterized by FTIR, ^1H NMR, and UV-vis.

Lysine-dopamine (LDA) was synthesized from L-lysine HCl (LYS) and dopamine HCl, as reported in the literature.¹¹ LDA was utilized to obtain PU-LDA, allowing the chain extension, and lysine was used for PU-LYS as the control group for comparison.

The PUs were synthesized similarly to how reported elsewhere,²¹ and a scheme of the synthesis is reported in Figure 1a. In particular, the triblock copolymer PCL-PEG-PCL was dissolved in anhydrous DMF in a round-bottom flask; then 1,4-diisocyanatobutane (BDI) was added, and the reaction was carried out for 2 h at 70 °C under argon in the presence of $\text{Sn}(\text{Oct})_2$ as catalyst. Then, the chain extenders LYS or LDA were dissolved in anhydrous DMF, and DEA was added. This solution was added dropwise into the reaction round-bottom flask and carried out at 25 °C for 20 h. The product was purified by dropwise precipitation in cold diethyl ether under stirring and washed 4 times in 2-propanol. Finally, the product was dried under vacuum, resulting in a white powder for PU-LYS and a pink powder for PU-LDA. The stoichiometry of the reagents was set at 1:2.3:1 of PCL-PEG-PCL:BDI:LYS/LDA. Polyurethanes were characterized by FTIR, ^1H NMR, SEC, and DSC. The amount of dopamine inserted on the PU-LDA derivative was quantified by UV-vis by using LDA as a standard.

2.4. Film Casting Procedure, Hydrolysis Studies, Swelling, and Contact Angle Measurements. The synthesized polymers were dispersed in chloroform at room temperature (30% w/v). The solutions were poured onto polytetrafluoroethylene (PTFE) molds and allowed to dry at room temperature inside a drier. Initial solution volumes were selected to obtain a 0.5 mm thickness of PU films. The hydrolysis study on polyurethane films produced by film casting was

carried out in DPBS pH 7.4, with 0.02% of sodium azide, at 37 °C in a 48-well plate placed inside an incubator. Polyurethane films produced by film casting were cut into 1 cm^2 disks, washed in distilled water, lyophilized, and weighed (W_0). The solution was replaced weekly, and the weight loss was measured at scheduled time intervals of up to 6 months. At each time point, the samples were washed 4 times in ultrapure water and lyophilized. The hydrolysis experiments were performed in triplicate, and the results were expressed as the mean value of the recovered weight \pm standard deviation. Results were plotted against t_0 .

The swelling ability of the films was tested after incubation in DPBS pH 7.4 for up to 14 days in a 48-well plate placed inside an incubator. Polyurethane films produced by film casting were cut into 1 cm^2 disks and weighed (W_0). At each time point, films were withdrawn and weighed after gently removing the liquid that covered the external surface with soft filter paper. To quantify swelling behavior, the swelling ratio was calculated using the following equation

$$\text{Swelling ratio} = \frac{(W_s - W_0)}{W_0} \times 100$$

where W_0 is the dry weight of the polymeric films and W_s denotes the weight of films after swelling. Each experiment was performed 5 times.

The hydrophilic behavior of the polyurethanes was analyzed by contact angle measurements. Deionized water was dropped onto the surfaces of both PU-LYS and PU-LDA, and an image of the drop was recorded. The software was used to calculate the contact angle at scheduled time intervals of up to 10 min. The contact angle experiments were performed in triplicate at room temperature, and results were expressed as the mean value \pm standard deviation.

2.5. Cytocompatibility Studies. Human dermal fibroblasts-adult (NHDF-Ad) were obtained from Lonza Bioscience and used after 7 doublings. The cell line was grown in the minimum essential medium DMEM supplemented with 10% (v/v) fetal bovine serum (FBS), 2 mM L-glutamine, 100 U/mL penicillin, 100 $\mu\text{g}/\text{mL}$ streptomycin, and 2.5 $\mu\text{g}/\text{mL}$ amphotericin B (all reagents were from Euroclone, Milan, Italy) under standard conditions (95% relative humidity, 5% CO_2 , 37

°C). The cells were seeded in flasks at 2.5×10^4 cells/cm² and allowed to grow until confluence.

Films produced as described in paragraph 2.4 were sterilized with 75% alcohol and ultraviolet light irradiation. Then, they were transferred into a 48-well tissue culture polystyrene plate, and 500 mL of cell suspension (about 30 000 cells per well) was used for culture seeding.

Indirect cell viability in the presence of PUU disks was assessed by a 3-(4,5-dimethylthiazol-2-yl)-5-(3-carboxymethoxyphenyl)-2-(4-sulphophenyl)-2H-tetrazolium (MTS) assay, using a commercially available kit (CellTiter 96 Aqueous One Solution Cell Proliferation Assay, Promega) containing MTS and phenazine methosulfate (PMS).

At each time point, the supernatant was removed, and each well was washed with sterile DPBS. After this, cells in each well were incubated with 500 μ L of fresh DMEM and 100 μ L of an MTS solution, and plates were incubated for 2 h at 37 °C. 100 μ L aliquot of the solution in each well was transferred into a 96-well flat plate. The absorbance at 490 nm was read by using a Microplate reader (Multiskan Ex, Thermo Labsystems, Finland). Relative cell viability (percentage) was expressed as (Abs₄₉₀ PU-LDA cells/Abs₄₉₀ PU-LYS cells) \times 100, based on three experiments conducted in multiples of four. Cells incubated with the medium were used as a negative control.

Moreover, acridine orange/ethidium bromide (AO/EB) double staining was performed to confirm the MTS results.

Direct cell viability was performed in triplicate by directly seeding cells (5×10^4 , 50 μ L) on PUU disks in a 48-well plate. After 30 min, 500 μ L of DMEM was added, and cells were cultured for 7 days. The discs were then washed with DPBS and stored in 4% formaldehyde for 30 min at 4 °C. Dehydration was performed with mixtures containing increasing amounts of ethanol (15, 30, 50, 75, and 100%), and the films were stored in the dryer until SEM analysis.

2.6. Adhesion Evaluation. **2.6.1. Tack Test.** Tack test measurements were performed with a DHR-2 TA Instruments rotational rheometer with a Peltier plate cartridge using a 20 mm upper plate. For tack test adhesive strength experiments, PU-LDA obtained by film casting was placed between the bottom and the upper plate and kept at 55 °C for 15 min until a complete melting occurred. The gap was set at 300 μ m, and following a conditioning period of 60 s at 37 or 25 °C, it was linearly increased up to 450 at 0.5 μ m/s. These tests were all performed in tension mode to evaluate the tendency of these materials to form a connection to a substrate after melting. All measurements were performed at 37 and 25 °C in triplicate, and results were expressed as the mean value.

2.6.2. NIR-Induced Film Fusion Procedure and Lap Shear Tests. Lap-shear experiments were conducted on aluminum, glass, polypropylene, and porcine skin at room temperature and dry conditions to evaluate adhesive strength. Further tests were conducted on porcine skin in wet conditions and at 37 °C submerged in water to evaluate the interaction with biological tissue. Each specimen was cut into a rectangular shape, 7.50 cm long and 2.5 cm wide. As a general procedure to allow the PU-LDA to melt, an NIR irradiation procedure was applied. The PUU films were weighted, placed onto the specimen, and irradiated with a NIR laser from a distance of 15 cm until melting occurred. PU-LDA required less than 60 s at 4 W/cm² and PU-LYS 7.5 W/cm² for 120 s. The film (1 cm²) was first fused by NIR irradiation on the surface of a single porcine skin specimen, and then a second specimen was rapidly overlapped 2.5 cm in a lap shear configuration with the specimen where the PU was fused, and 200 g weight was placed on top of them for 5 min. For dry measurements, no further preparation was needed, and mechanical testing was performed by tensile measurements. The wet condition was made by submerging in DPBS for 2 min the overlapped porcine skin. The analysis at 37 °C was conducted by submerging the overlapped porcine skin already mounted on the heated tensile system. The load was incremented stepwise until failure occurred. The adhesive strength was obtained by dividing the maximum load (N) observed by the area of the adhesive overlap (m²), giving the lap-shear adhesion in pascal (Pa = N/m²). These

experiments were performed in triplicate, and results were expressed as the mean value \pm standard deviation.

2.7. Rheology. To perform rheological studies, a DHR-2 TA Instruments rotational rheometer with a Peltier plate cartridge and 20 mm upper plate was used. PU-LDA films obtained by solvent casting were used for the analysis. Before carrying out each experiment, the sample was conditioned for 60 s at the analysis temperature. The flow sweep experiment was conducted by applying a range from 0.01 to 100 s⁻¹. The time sweep measurements were conducted at a constant temperature, constant strain (1%) and constant frequency (10 rad/s) for 600 s. All these analyses were performed at constant temperatures of 80, 75, 70, and 65 °C. Moreover, the time sweep measurements were conducted in 2 steps by applying a constant strain of 1% and a constant frequency of 10 rad/s. The first step was at 80 °C for 120 s, and the second step was at 37 °C for 1200 s.

The measurement gap was set at 200 μ m for all analyses. All experiments were conducted in triplicate using a 20 mm parallel plate, and results were expressed as the mean value.

Thermo-rheological experiments were conducted in 2 steps: cooling down the sample from 80 to 25 °C and after heating it again to 80 °C at a rate of 1 °C/min by applying a constant strain of 1% in the linear viscoelastic region and a frequency of 10 rad/s.

2.8. 3D Printing Processing. PU-LDA was melted at 80 °C inside a heat-controlled print head equipped with a 23-gauge needle to produce 300 μ m filaments. The deposition was performed with a constant pressure of 75 psi on a heated glass surface at 50 °C. We chose two different patterns to evaluate different fiber diameters and shape fidelity to the digital model.

2.9. Statistical Analyses. All reported values are means with error bars corresponding to the standard deviation. A paired sample Student's *t*-test was used to identify differences in lap shear tests. Two-way ANOVA was performed on the porcine skin experiments in lap shear configuration. Statistical significance was determined by *p*-values < 0.001.

3. RESULTS AND DISCUSSION

3.1. Synthesis and Characterization of PU-LDA. The triblock copolymer PCL-PEG-PCL was synthesized by ring-opening polymerization from ϵ -CL and PEG with a yield above 95% as reported in the literature.²¹ Both of them are widely used for biomedical applications due to their excellent biocompatibility.¹⁷¹⁸¹⁹²⁰²¹ Furthermore, PEG has a low melting temperature ($T_m \sim 38$ °C), and we have chosen the molar ratio between them consequently to achieve a melting temperature of around 55 °C. The ¹H NMR spectra, reported in Figure S1, showed the characteristic peaks of methylene protons of PCL block, labeled as a, b, c, and d, at 1.4, 1.7, 2.3, and 4.3 ppm, respectively, while the ethylene oxide protons of PEG, labeled as e, were displayed at 3.7 ppm. The sum of all PCL peak contributions is 3.17 times higher than the PEG peak, and since the PCL peaks are due to 10 protons and PEG to 91, the resulting molar ratio is 29. The macromolecular weight ($M_n \sim 4300$) and PEG/PCL block ratios estimated from the ¹H NMR spectrum were consistent with the theoretical value calculated from the feed ratio.

Lysine-dopamine LDA was synthesized from L-lysine HCl and dopamine-HCl, as reported in the literature.¹¹ The structures of LDA and intermediate products were confirmed by FTIR, ¹H NMR, and UV-vis spectroscopy (see Supporting Information Figure S2). It is a functional biomolecule containing a mussel-derived adhesive moiety (catechol) and a biofunctional moiety (lysine). Moreover, the primary amine groups of lysine residue have particularly high reactivity with the isocyanate group to act as a chain extender on polyurethane urea's synthesis. Both polyurethanes were synthesized using the triblock copolymer PCL-PEG-PCL

as a soft segment and 1,4-diisocyanatobutane as a hard segment. LDA was utilized to obtain PU-LDA, allowing the chain extension, and lysine was used for PU-LYS as the control group for comparison (Figure 1a).

The ^1H NMR spectra of the two polyurethanes (PU-LDA and PU-LYS) (Figure 1b) showed the same characteristic peaks of PCL–PEG–PCL between 1.4 and 4.3 ppm. Comparing the PU-LDA and PU-LYS spectra, it is possible to highlight the presence of peaks between 6.65 and 7.00 ppm attributable to the 3 protons of aromatic CH. In the UV–vis spectrum of LDA (Figure 1c), there is an absorbance peak for the catechol group at 280 nm, which confirms the conjugation of dopamine with lysine for the chain extender. This peak is present also in PU-LDA, confirming the presence of dopamine in the polyurethane. This information, combined with the previous ones obtained from FTIR, ^1H NMR, and SEC, confirms the success of the reported synthesis reactions. The amount of LDA bound to the PU-LDA was quantified through UV and is equal to 5.5% (w/w).

SEC analyses, reported in Table 1, showed that M_w increased significantly from PCL–PEG–PCL (5.7 kDa) to

Table 1. Molecular Weight Evaluation from SEC Analysis (M_n , M_w , and PDI) and M_n of PCL–PEG–PCL from ^1H NMR

	M_n ^1H NMR	M_n	M_w	PDI
PCL–PEG–PCL	4300	5 600	5 700	1.1
PU-LDA		41 900	51 600	1.2
PU-LYS		23 700	45 100	1.9

PU-LYS (45.1 kDa) and PU-LDA (51.6 kDa). This result demonstrates the successful polymerization process and is coherent with the previous results.²¹ The structures of the whole synthesis were also confirmed by FTIR (Figure S3).

The thermal behavior of selected polyurethanes was studied by TG–DSC analyses (Figure 2a). Figure 2b clearly shows two different melting temperatures of polyurethanes. The first one at 38 °C is correlated to the PEG block, and the other at 56 °C is due to the PCL. A glass transition temperature (T_g) was observed at −17 °C. The PU-LDA exhibited soft segment

transitions over the temperature range of −50 to +150 °C, and the absence of a hard segment transition agreed with results detected for similar PUs.²¹

Figure 2c highlights the absence of degradation <325 °C, which allows melting of the material to process it.

To characterize properties of the polymer like degradation rate, cytocompatibility, adhesiveness after melting, and viscosity, the polyurethanes were processed as films by the film casting procedure.

Hydrolytic degradation was measured in sodium azide/DPBS at 37 °C over 6 months. The results reported in Table 2 showed that the amount of mass lost is always <4%, which is consistent with previous studies since PCL degrades very slowly.²² This result underlines the synthesized PU's remarkable hydrolytic resistance, which is a fundamental design requirement for tissue-engineered scaffolds to maintain structure and function over time (Table 3).

The swelling analysis did not show significant differences between the PUUs for each time point up to 14 days. The slightly higher swelling values for PU-LYS could be attributable to the free carboxyl group that can interact with water.²³

The water contact angle of the films (Figure 3) started at 61° for PU-LDA and 71° for PU-LYS and both decreased to 37 and 53°, respectively. The small difference between the two polymers can be attributed to the presence of the catechol group that increases hydrophilicity. Hydrophilic polymers perform better as bioadhesives because they can form strong bonds with highly hydrophilic tissues.¹

The cell viability of NHDF in the presence of PU disks was assessed by an MTS assay for up to 7 days. The results showed no significant difference between the polyurethane, and the viability was >96% at each time point. Therefore, we can assume the absence of cytotoxic degradation products for both PUU derivatives (Figure 4a).

These data were also confirmed by acridine orange/ethidium bromide (AO/EB) double staining. According to fluorescence emission, it is possible to distinguish viable cells from apoptotic and necrotic cells. Indeed, acridine orange is taken up by both viable and nonviable cells, emitting green and red fluorescence if intercalated with double-stranded nucleic acid (DNA) and single-stranded nucleic acid (RNA),

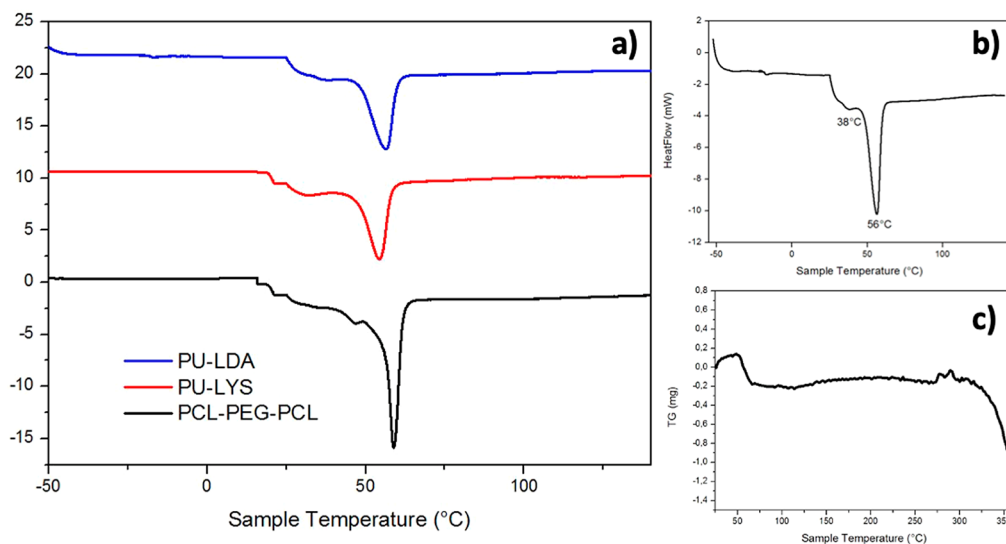


Figure 2. (a) DSC comparison between synthesized products, (b) DSC details of PU-LDA, and (c) thermal degradation of PU-LDA.

Table 2. Residual Mass (R_m) % after Hydrolytic Degradation over 6 Months

time (weeks)	0.7	1.4	3	5	9	13	17	21	25
R_m (%) PU-LDA	98 ± 0.7	99 ± 1	98 ± 0.5	98 ± 0.5	97 ± 0.5	96 ± 3	99 ± 2	96 ± 1	97 ± 1

Table 3. Swelling Ability of the PUU Films Tested after Incubation in DPBS pH 7.4 for up to 14 Days at 37 °C

swelling (%)	1 day	7 days	14 days
PU-LDA	18.4 ± 0.9	18.3 ± 1.2	18.4 ± 1.2
PU-LYS	17.6 ± 1.2	20.5 ± 0.8	20.1 ± 1.1

respectively. Instead, ethidium bromide is taken up only by nonviable cells and emits red fluorescence through intercalation within the DNA. Viable cells appear with a uniformly bright green nucleus and orange cytoplasm. Even early apoptotic cells have green nuclei, but in this case, it is possible to note a perinuclear chromatin condensation as bright green fragments. Orange to red nuclei with condensed or fragmented chromatin are visible to late apoptotic cells, while necrotic cells have uniformly orange to red nuclei with organized structure.²⁴

As shown in Figure 4b, most cells were viable for up to 7 days, and no significant apoptosis was detected, with only a few dead cells found.

The cytocompatibility was further confirmed by the direct culture of cells on PU-LDA films. SEM images (Figure 4c) showed that cultured fibroblasts maintained their typical shape and morphology after 7 days of culture, showing elongation and complete integration within the PUU matrix. This preliminary data conceivably suggests the optimal cytocompatibility of synthesized polymers and the cell-adhesive properties of PU-LDA films.

3.2. Adhesion Evaluation. The adhesive behavior of PU-LDA was preliminarily assessed by tack test analysis, and the results are reported in Figure 5a,b. The tackiness of materials, which depends on the cohesive forces between the adhesive itself and the substrate, is associated with stickiness and may result from adhesive or cohesive forces between two materials in contact or a material bridging two substrates. The tack is then recorded as the maximum force required to break the resultant bond, describing the tendency of materials to form a connection to a substrate. Here, PU-LDA film was subjected to a tack test to measure its adhesive properties as a function of

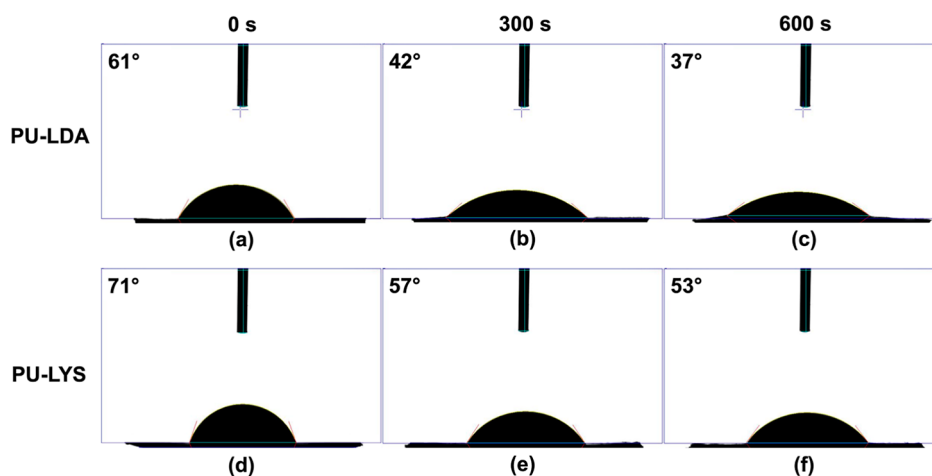
temperature, recording the minimum force and the tackiness of the material expressed as the area under the force–time curve.

The gap (red line) and axial force (black line) profiles for PU-LDA are shown in Figure 5a,b. These graphics show a reduction in compressive force with a residual tensile (negative) force, corresponding to tack and adhesion of the material, at 37 °C (Figure 5a) or 25 °C (Figure 5b) after the gap (μm) was raised linearly at 0.5 $\mu\text{m/s}$.

When the experiments were performed at 37 °C, the time failure, which corresponds to the time for the force to decay by 90% of peak values (13 N), was 75 s. This preliminary result demonstrated that the adhesive potential of PU-LDA can be exploited only once the polymer is melted and in contact with the specific surface. Once it is fused, the molecular interactions between the adhesive and the material can occur, and then when the material is cooled under the melting point, the adhesive interactions can be exploited. At 25 °C, the force reached higher values with no failure observed and a gap constant at 317 μm . Cooling the material from 37 to 25 °C caused an increment of adhesion of the sample. This qualitative analysis suggests that the PU-LDA film can exploit its adhesiveness after low-temperature melting (55 °C) and cooling at 37 and 25 °C.

The quantitative evaluation of bonding strength is usually evaluated through tensile tests until detachment of the adherent specimens. If the failure occurs within the adhesive layer, it is considered a cohesive failure, instead, if it occurs at the interface with one of the specimens, it is an adhesive failure. The adhesion force of PU-LDA was examined in lap shear configuration and compared with that of the control group PU-LYS. Indeed, it has been the most often used adhesion bonding test among the several existing methods for evaluating adhesives.^{9,25,26}

We chose four materials to evaluate the adhesion of PU-LDA and used PU-LYS as the control group. Lap shear results for all surfaces and conditions tested are provided in Figure 5c. Aluminum and glass are high-energy surfaces, and the resulting adhesion is considerably higher (respectively 2600 ± 150 and 2836 ± 462 kPa for PU-LDA and 720 ± 103 and 1237 ± 47

**Figure 3.** Determination of the contact angle on PU-LDA (a–c) and PU-LYS (d–f) films: images acquired after 0, 300, and 600 s.

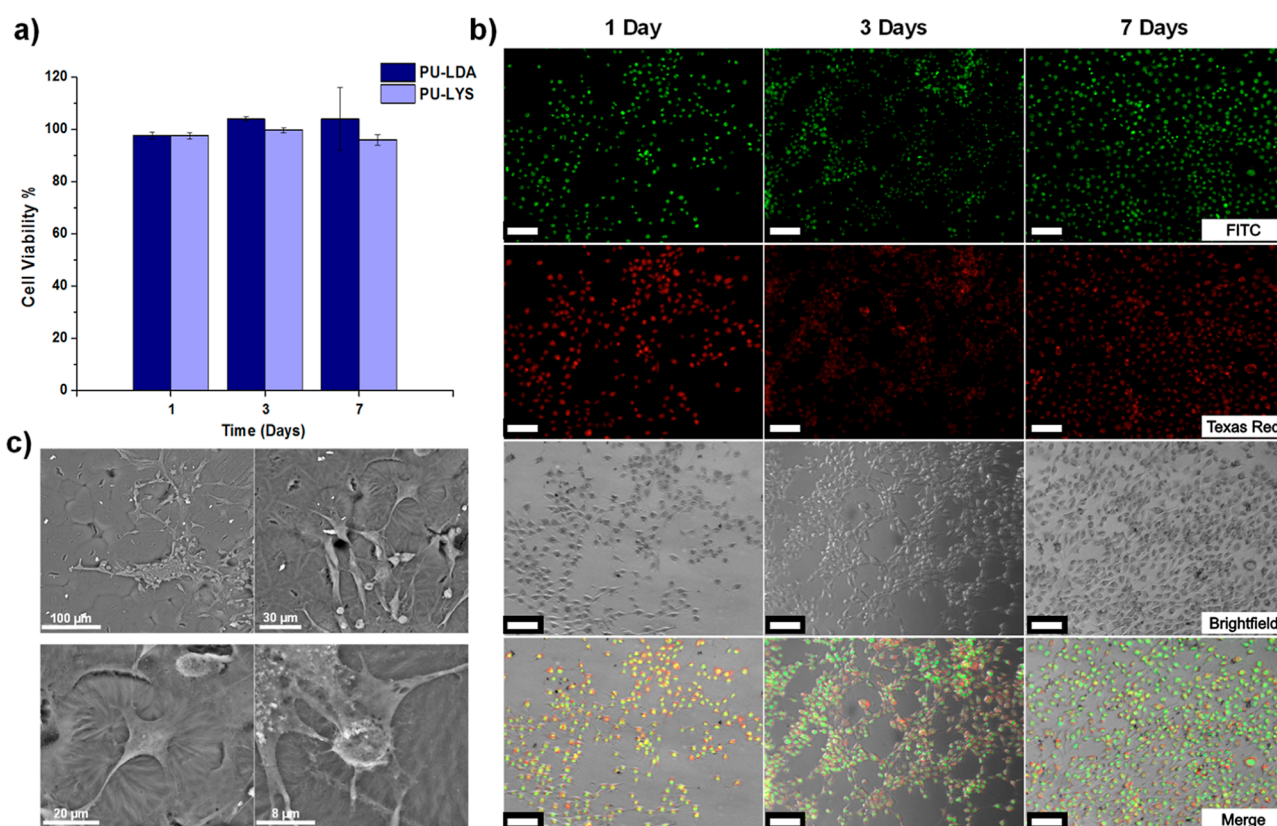


Figure 4. (a) Indirect viability comparison between PU-LDA and PU-LYS; (b) fluorescence images of NHDF cells stained with acridine orange/ethidium bromide (AO/EB) double staining after 1, 3, and 7 days of culture with PU-LDA films (indirect cell viability) 100 μm scale bar; (c) SEM images of cells growing in direct contact with PU-LDA films after 7 days of culture.

kPa for PU-LYS) than low-energy surfaces like polypropylene (306 ± 17 kPa for PU-LDA and 194 ± 14 kPa for PU-LYS). These differences between high- and low-energy surfaces could be attributable to hydrogen bonding or polar interactions since the polymers have a relatively large polar component and ester/urea bonds.²⁶ Instead, the effect of dopamine bonded to the chain extensor is remarkable, and the increase in adhesion strength is $>100\%$ when compared with the control group (PU-LYS) for aluminum, $\approx 200\%$ for glass, and $>50\%$ for polypropylene.

Lap shear adhesion tests were also performed on porcine skins to evaluate the adhesive's possible applications on biological tissues (Figure 5d). With their biological similarity to the human dermis, porcine skins are commonly used for biomedical experiments.^{26,27} A NIR irradiation procedure was set up to achieve a fast and spatially controlled melting of PU to allow for the exploitation of adhesiveness on biological tissues (Figure 5e). NIR irradiation can be a fast and efficient procedure to localize specific areas of melting on the PU-LA biomaterials when it is applied on a tissue surface. Low laser intensity for fast irradiation times is sufficient to allow complete fusion of the material with efficient spatial control (Figure S4).

Applying the NIR-mediated melting procedure, a classical lap shear configuration was prepared.

We observed that dopamine remarkably increases the adhesiveness of polyurethane in every tested condition. In dry conditions, the adhesion strength of PU-LDA is 50 ± 4 kPa, which is 100% higher than that of PU-LYS (26 ± 3.6 kPa). The difference increases even more when water is

involved, 150%, indeed, after 2 min of immersion in DPBS, the adhesion strength of PU-LDA decreased to 40 ± 3.8 and that of PU-LYS to 13.53 ± 1.6 . Lastly, when the experiment was performed underwater at 37°C , PU-LDA decreased to 28.2 ± 0.6 kPa, which is 150% higher than PU-LYS equal to 9.5 ± 1.4 kPa.

Adhesive failure was observed for all tested samples, indicating a stronger cohesive strength than adhesion. Overall, all the presented adhesion results are consistent with the literature on lap shear configuration. Zhou et al. synthesized a poly(ester-urea)-based degradable adhesive polymer, inspired by mussel adhesive proteins, using interfacial polycondensation. They have demonstrated that their polymer has an adhesion strength, without an oxidative cross-linker, of 1000 kPa on aluminum adherents and 3 kPa on porcine skin.²⁶

Xu et al. have designed a stretchable biointerfacial electrode based on a highly adhesive elastomer that contains dopamine as a pendant group suitable for electromyogram measurement. It exhibits an underwater adhesive strength equal to 16 kPa with epithelial tissue.²⁷

Matos-Pérez et al. observed a 1.3 ± 0.2 MPa adhesion strength to aluminum with their 10% catechol and 90% styrene copolymer.²⁵

The main advantage of our polyurethane, although our results showed higher performances than those of the cited works, is that it is a solid processable material capable of expressing high adhesion to different substrates and in different conditions after melting occurs. Indeed, it does not require the use of organic solvents to be spread properly on the target and can be processed to obtain precise and defined microfibers and

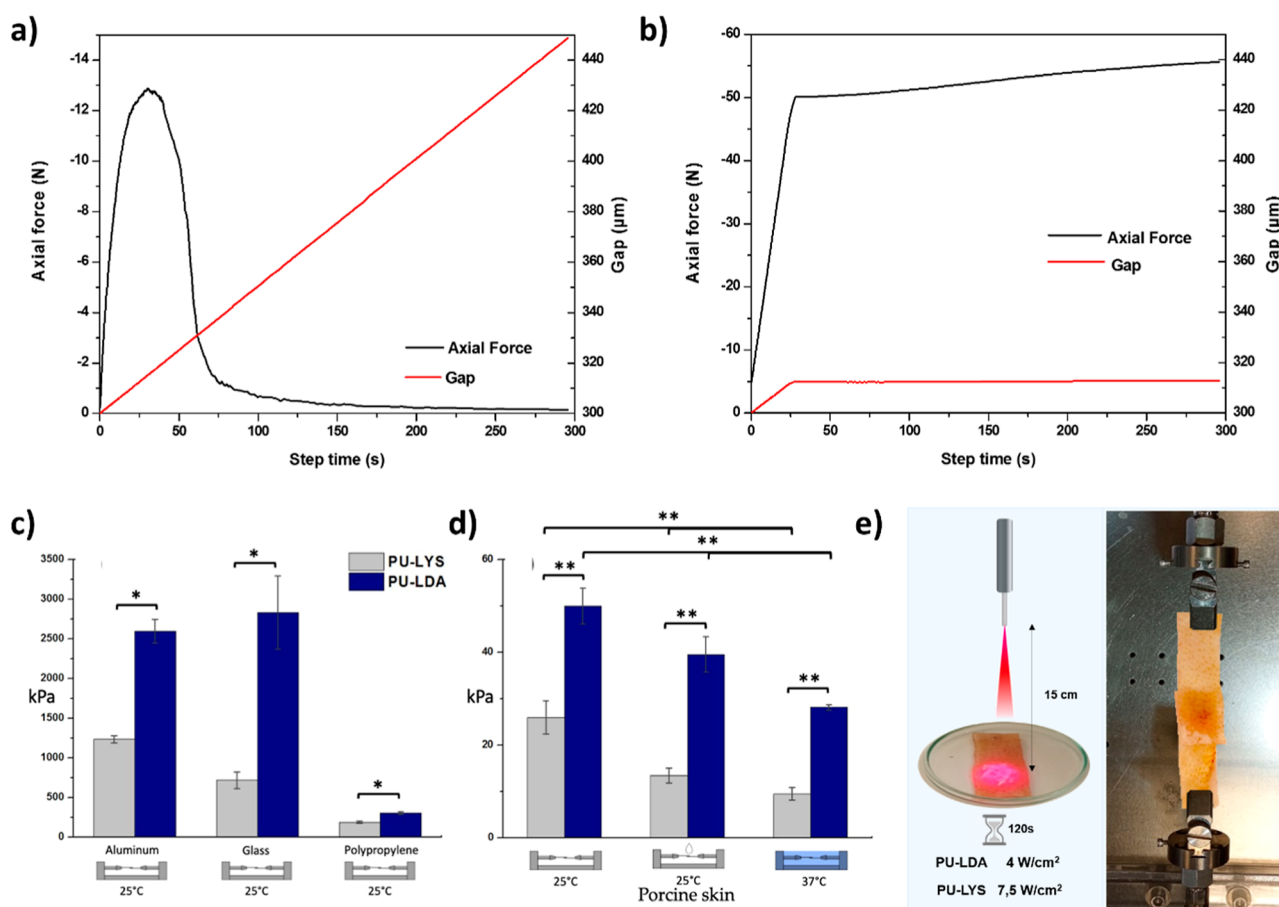


Figure 5. Force (N) versus time curves of PU-LDA film obtained in the Tack test at 37 (a) and 25 °C (b); (c) lap shear results at room temperature and dry conditions, *t*-test (2:2) $P < 0.001$, (d) lap shear results on porcine skin adherents respectively at 25 °C and dry conditions (left), 25 °C and wet conditions (middle), 37 °C submerged in water, two-way ANOVA $P < 0.001$; (e) phases of the lap shear test: NIR-induced film fusion by laser NIR irradiation for 120 s; adhesion of the two specimens of skin; immersion in DPBS; evaluation of the lap-shear adhesive strength by Bose TA Instruments ElectroForce Test Bench System.

to build up structures with a tunable microarchitecture and external shape. Furthermore, it does not require cross-linkers or oxidants to express high adhesion. To express high adhesion, PU-LDA can either be premelted by simple fusion or, once applied as a solid on the surface to be attached, by precise spatial control by laser irradiation. These conditions, for instance, are ideal for wearable devices that require a stimulus-sensitive adhesive interface between the sensor and the skin.

3.3. Rheological Analyses of PU-LDA and 3D Printing Procedure. Material rheological properties are the most critical parameters for extrusion 3D printing of melted polymers.^{28–30} Rheology influences the melt temperature and helps determine the material output and flow rate by predicting the material flow and required pressure through the nozzle during the process. In melt extrusion 3D printing, both temperature and shear rate strongly affect the deformation behavior and melt viscosity, which represent the most important parameters in determining the optimal processing conditions. Viscosity decreasing with increased shear rate can be associated with shear thinning behavior, which is favored melt extrusion 3D printing applications, as this means the ability of the material, at a given temperature, to be easily pushed through a nozzle but also to maintain the given structure and shape after deposition due to the initial viscosity value recovered as pressure is removed.³¹ Studying the optimal

viscosity range can help in predicting the material suitability in the 3D printing process. A high value of zero-shear viscosity at a low shear rate could help to maintain the shape after deposition. Instead, viscosity data at high shear rates are more representative of the rheological properties of the materials during extrusion. Indeed, it has to be low for efficient printing, but at the same time, it should not be so low that it flows as liquid from the printing nozzle.³²

As shown in Figure 6a, PU-LDA, tested at 80, 75, 70, and 65 °C, showed shear thinning behavior at all tested temperatures with values ranging between 10^4 and 10^5 Pa s at a low shear rate (0.01 s^{-1}) down to 10^2 Pa s at 100 s^{-1} , with more than 2 orders of magnitude difference, which agrees with previous studies suggesting that printable polymeric systems are in the range 10–1000 Pa s at high shear rate.^{28,33}

However, at a fixed temperature and deformation, melted materials have to keep constant their storage (G') and loss modulus (G''), such as their viscosity values; if not, it might be necessary to change printing parameters during printing with negative repercussions on the success of the extrusion process. Time sweep analyses were performed at different temperatures, keeping constant strain and angular frequency, to evaluate this aspect. It is possible to note that complex viscosity (in the order of 10^2 Pa s) and both G' and G'' (in the order of 10^3 Pa) were constant up to 600 s, and values increased as temperature decreased from 80 to 65 °C (Figure 6b,c). The higher the

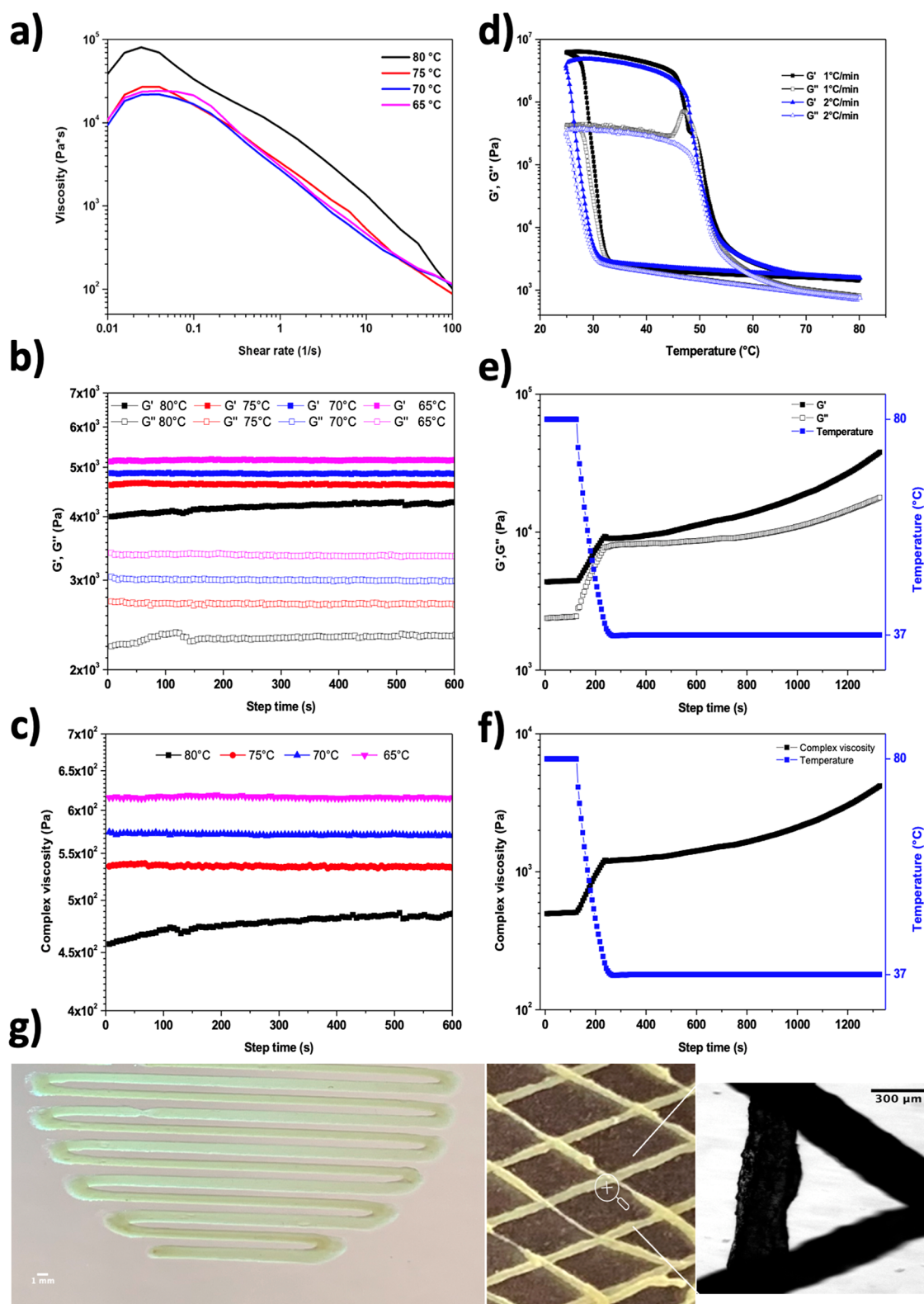


Figure 6. (a) Flow sweep analysis, (b) time sweep analysis with moduli versus time at 80, 75, 70, and 65 °C of PU-LDA, (c) complex viscosity during time sweep at constant temperatures, (d) temperature ramp analysis (80–25 °C) and back (25–80 °C) at 1 °C/min, (e) time sweep analysis with moduli versus time at 80 °C for 120 s and at 37 °C for 1200 s, (f) complex viscosity during time sweep after temperature variation. (g) Printed patterns of PU-LDA and microfiber detail.

modulus and viscosity, the more difficult the flow, resulting in nozzle clogging. However, as values are too low, it can result in a leakage of material from the nozzle.³⁴ Thus, material rheological properties are dependent on the temperature,

which is another crucial factor to not overlook. Rheological investigation results show that the viscosity and moduli values of PU-LDA are in a range that is well suited for processing by the melt extrusion 3D printing technique.³⁵

In the melt-extrusion setting, the correct temperature can change the printing outcome. High print temperatures can determine the too-low viscosity of the polymer with consequently flow instability. On the other hand, low processing temperatures can determine points of failure and defects due to incomplete polymer melting.^{36,37} The temperature ramp rheogram (Figure 6d) showed how G' and G'' strongly depend on changing temperatures. This and the tack test measures highlight PU-LDA's broad adhesive working temperature range. Indeed, after melting occurs, it is possible to express high bioadhesion even at 37 °C to avoid any undesired effect due to the temperature difference when applied to tissues. As temperature decreased from 80 to 25 °C, moduli increased with a drastic jump at 33 °C of about 4 orders of magnitude, reaching, at 25 °C, 6×10^6 and 4×10^5 Pa for G' and G'' , respectively, showing a more structured material at this temperature. As the temperature increased again up to 80 °C, moduli gradually decreased up to 46 °C, and at this temperature, they dropped immediately reaching 1.5×10^3 and 8×10^2 Pa for G' and G'' , respectively, at 80 °C. Data are in accordance with DSC results.

Another aspect to consider in the melt-extrusion 3D printing process is the capacity of the deposited layer to adhere to the subsequent layer. This aspect determines the final of the 3D printed construct with weak mechanical properties if poorly adhered layers occurred. Both viscosity and temperature play another key role in filament coalescence.³⁸ To better predict shape fidelity to the digital model, moduli and viscosity have to quickly recover their values after deposition. Ideally, the temperature should be high enough to ensure adhesion between successive layers but at the same time able to support deposition and consequently the structural integrity of the printed construct. Thus, time sweep analyses (Figure 6e,f) were performed to study the time to get an increment of G' , G'' , and the complex viscosity of the material as temperature decreased. As the temperature dropped from 80 to 37 °C, all values sharply increased by half an order of magnitude, while, as the temperature was constant at 37 °C, the values gradually increased up to 3.8×10^4 Pa and 4×10^3 Pa s for G' and complex viscosity, respectively, after ~1320 s. The quick and incomplete increase of these values may enable the layer's deposition; however, these values can allow layers adhesion thanks to the gradual increase over time.

The melt extrusion 3D printing study, reported in Figure 6g, aimed to assess the feasibility of generating various fiber diameters and maintaining shape fidelity to the digital model through the implementation of two distinct patterns. Both patterns were reproduced with high accuracy, even when the nozzle traversed narrow curves. Melt-extrusion 3D printing, used to produce oriented microfibers, involves the heating and extruding of the polymer through a nozzle tip. The fibers are deposited on a heated build plate forming a specific pattern. The remarkable adhesion strength could allow us to produce adhesive coating patterns on inorganic metallic materials, providing a structured interface that facilitates cellular attachment, promotes tissue growth, and improves long-term biocompatibility. Indeed, the presence of specific micro-patterns, such as lines, dots, or pits, can guide cell adhesion, spreading, and alignment. These micropatterned coatings promote focal adhesion formation, cytoskeletal rearrangement, and enhanced cell–substrate interactions, ultimately leading to improved tissue integration. The main concern about this technique is the potential degradation due to the high

temperature. Indeed, in most of the literature, it is set in a range between 150 and 230 °C.³⁹ However, thanks to the low melting point of PU-LDA, we could able to perform this process at <80 °C. Furthermore, thanks to the results over time observed from the rheological time sweep analysis, we were able to perform the melt-extrusion processing with a constant pressure of 75 psi. Lastly, the quick recovery in moduli and complex viscosity by half an order of magnitude when the temperature dropped from 80 to 37 °C helped us better predict shape fidelity to the digital model.

4. CONCLUSIONS

In the present study, we have synthesized, characterized, and processed a biodegradable segmented polyurethane as a biomaterial. BDI was used as a reactive for the generation of hard segments following the chemistry of isocyanates, and LDA as a dopamine-containing chain extender. This polyurethane urea has a remarkable hydrolytic resistance to degradation, a low melting point (55 °C), and high adhesion. These properties suit well the use of this polyurethane urea as a coating interface between metallic prostheses or implantable devices and biological tissues to improve biological tolerance and improve biointegration.

Moreover, the low melting temperature of about 55 °C and the rheological properties of the melted polymer suggest the good suitability of the PU-LDA for the melt-extrusion 3D printing procedure, allowing the production of precise microfibers and building up structures with a tunable microarchitecture and external shape. The shown high adhesion and processability open several interesting applications for this biomaterial, such as micropattern coatings on implantable devices or drug delivery systems, since it could incorporate even thermolabile drugs or biomolecules. Moreover, the incorporation of an electroactive component could extend the possible application to implantable sensor devices.

■ ASSOCIATED CONTENT

Supporting Information

The Supporting Information is available free of charge at <https://pubs.acs.org/doi/10.1021/acsapm.3c01578>.

Additional experimental details include ¹H NMR of the synthesized block copolymer; scheme of LDA synthesis with ¹H NMR, FT-IR analysis, and UV–vis; FT-IR analysis of the block copolymer compared with synthesized polyurethane ureas; and spot melting detail of the product (PDF)

■ AUTHOR INFORMATION

Corresponding Author

Fabio Salvatore Palumbo – Dipartimento di Scienze e Tecnologie Biologiche Chimiche e Farmaceutiche (STEBICEF), Università degli Studi di Palermo, 90123 Palermo, Italy; orcid.org/0000-0001-6196-7782; Email: fabiosalvatore.palumbo@unipa.it

Authors

Giovanni Carlo Miceli – Dipartimento di Scienze e Tecnologie Biologiche Chimiche e Farmaceutiche (STEBICEF), Università degli Studi di Palermo, 90123 Palermo, Italy; orcid.org/0000-0002-1895-8343

Annalisa Martorana – Dipartimento di Scienze e Tecnologie Biologiche Chimiche e Farmaceutiche (STEBICEF),

Università degli Studi di Palermo, 90123 Palermo, Italy;

orcid.org/0000-0002-5307-2476

Francesco Cancilla – Dipartimento di Scienze e Tecnologie Biologiche Chimiche e Farmaceutiche (STEBICEF), Università degli Studi di Palermo, 90123 Palermo, Italy; orcid.org/0000-0002-8453-0804

Giovanna Pitarresi – Dipartimento di Scienze e Tecnologie Biologiche Chimiche e Farmaceutiche (STEBICEF), Università degli Studi di Palermo, 90123 Palermo, Italy; orcid.org/0000-0002-0815-9142

Mariano Licciardi – Dipartimento di Scienze e Tecnologie Biologiche Chimiche e Farmaceutiche (STEBICEF), Università degli Studi di Palermo, 90123 Palermo, Italy; orcid.org/0000-0003-4539-9337

Complete contact information is available at:

<https://pubs.acs.org/10.1021/acsapm.3c01578>

Author Contributions

Giovanni Carlo Miceli: conceptualization, methodology, validation, formal analysis, investigation, data curation, writing—original draft, and visualization. Annalisa Martorana: methodology, validation, formal analysis, investigation, data curation, writing—original draft, and visualization. Francesco Cancilla: methodology, validation, formal analysis, investigation, data curation, writing—original draft, and visualization. Giovanna Pitarresi: resources, supervision, and funding acquisition. Mariano Licciardi: resources, supervision, funding acquisition, and writing—review and editing. Fabio Salvatore Palumbo: conceptualization, validation, resources, writing—review and editing, visualization, supervision, project administration, and funding acquisition.

Funding

The authors would like to thank MIUR for funding.

Notes

The authors declare no competing financial interest.

ACKNOWLEDGMENTS

The authors would like to thank ATeN Center of the University of Palermo—Laboratory of Preparazione e Analisi di Biomateriali, Laboratory of meccanica dei materiali e dei biomateriali, and the D'Amore Lab for providing access and assistance in the use of 3D printing equipment.

REFERENCES

- (1) Pandey, N.; Soto-Garcia, L. F.; Liao, J.; Zimmern, P.; Nguyen, K. T.; Hong, Y. Mussel-Inspired Bioadhesives in Healthcare: Design Parameters, Current Trends, and Future Perspectives. *Biomater. Sci.* **2020**, *8* (5), 1240–1255.
- (2) Zhu, W.; Chuah, Y. J.; Wang, D. A. Bioadhesives for Internal Medical Applications: A Review. *Acta Biomater.* **2018**, *74*, 1–16.
- (3) Lee, Y. J.; Son, H. S.; Jung, G. B.; Kim, J. H.; Choi, S.; Lee, G. J.; Park, H. K. Enhanced Biocompatibility and Wound Healing Properties of Biodegradable Polymer-Modified Allyl 2-Cyanoacrylate Tissue Adhesive. *Mater. Sci. Eng., C* **2015**, *51*, 43–50.
- (4) Ryssel, H.; Gazyakan, E.; Germann, G.; Öhlbauer, M. The Use of MatriDerm in Early Excision and Simultaneous Autologous Skin Grafting in Burns—A Pilot Study. *Burns* **2008**, *34* (1), 93–97.
- (5) Singer, A. J.; Quinn, J. V.; Hollander, J. E. The Cyanoacrylate Topical Skin Adhesives. *Am. J. Emerg. Med.* **2008**, *26* (4), 490–496.
- (6) Kirsch, M.; Ginat, M.; Lecerf, L.; Houël, R.; Loisanse, D. Aortic Wall Alterations after Use of Gelatin-Resorcinol-Formalin Glue. *Ann. Thorac. Surg.* **2002**, *73* (2), 642–644.
- (7) Hata, H.; Takano, H.; Matsumiya, G.; Fukushima, N.; Kawaguchi, N.; Sawa, Y. Late Complications of Gelatin-Resorcin-

Formalin Glue in the Repair of Acute Type A Aortic Dissection. *Ann. Thorac. Surg.* **2007**, *83* (5), 1621–1626.

(8) Hyon, S.-H.; Nakajima, N.; Sugai, H.; Matsumura, K. Low Cytotoxic Tissue Adhesive Based on Oxidized Dextran and Epsilon-Poly-L-Lysine. *J. Biomed. Mater. Res., Part A* **2014**, *102*, 2511–2520.

(9) Zhang, W.; Wang, R.; Sun, Z. M.; Zhu, X.; Zhao, Q.; Zhang, T.; Cholewinski, A.; Yang, F.; Zhao, B.; Pinnaratip, R.; Forooshani, P. K.; Lee, B. P. Catechol-Functionalized Hydrogels: Biomimetic Design, Adhesion Mechanism, and Biomedical Applications. *Chem. Soc. Rev.* **2020**, *49* (2), 433–464.

(10) Ribena, D. Dopamine Modification of Interfaces between Polymers and Metals. Ph.D. Thesis, Technische Universiteit Eindhoven, 2012.

(11) Sun, P.; Lu, H.; Yao, X.; Tu, X.; Zheng, Z.; Wang, X. Facile and Universal Immobilization of L-Lysine Inspired by Mussels. *J. Mater. Chem.* **2012**, *22* (19), 10035–10041.

(12) Hong, S.; Yang, K.; Kang, B.; Lee, C.; Song, I. T.; Byun, E.; Park, K. I.; Cho, S. W.; Lee, H. Hyaluronic Acid Catechol: A Biopolymer Exhibiting a PH-Dependent Adhesive or Cohesive Property for Human Neural Stem Cell Engineering. *Adv. Funct. Mater.* **2013**, *23* (14), 1774–1780.

(13) Jo, Y. K.; Choi, B. H.; Zhou, C.; Ahn, J. S.; Jun, S. H.; Cha, H. J. Bioengineered Mussel Glue Incorporated with a Cell Recognition Motif as an Osteostimulating Bone Adhesive for Titanium Implants. *J. Mater. Chem. B* **2015**, *3* (41), 8102–8114.

(14) Hauser, D.; Septiadi, D.; Turner, J.; Petri-Fink, A.; Rothen-Rutishauser, B. From Bioinspired Glue to Medicine: Polydopamine as a Biomedical Material. *Materials* **2020**, *13* (7), 1730.

(15) Suneetha, M.; Madhusudana Rao, K.; Soo Han, S. Mussel-Inspired Cell/Tissue-Adhesive, Hemostatic Hydrogels for Tissue Engineering Applications. *ACS Omega* **2019**, *4* (7), 12647–12656.

(16) Sun, P.; Wang, J.; Yao, X.; Peng, Y.; Tu, X.; Du, P.; Zheng, Z.; Wang, X. Facile Preparation of Mussel-Inspired Polyurethane Hydrogel and Its Rapid Curing Behavior. *ACS Appl. Mater. Interfaces* **2014**, *6* (15), 12495–12504.

(17) Mehdizadeh, M.; Weng, H.; Gyawali, D.; Tang, L.; Yang, J. Injectable Citrate-Based Mussel-Inspired Tissue Bioadhesives with High Wet Strength for Sutureless Wound Closure. *Biomaterials* **2012**, *33* (32), 7972–7983.

(18) Xu, J.; Tam, M.; Samaei, S.; Lerouge, S.; Barralet, J.; Stevenson, M. M.; Cerruti, M. Mucoadhesive Chitosan Hydrogels as Rectal Drug Delivery Vessels to Treat Ulcerative Colitis. *Acta Biomater.* **2017**, *48*, 247–257.

(19) Park, J. Y.; Yeom, J.; Seon Kim, J.; Lee, M.; Lee, H.; Sung Nam, Y.; Park, J. Y.; Kim, J. S.; Nam, Y. S.; Yeom, J.; Lee, M.; Lee, H. Cell-Repellent Dextran Coatings of Porous Titania Using Mussel Adhesion Chemistry. *Macromol. Biosci.* **2013**, *13* (11), 1511–1519.

(20) Fernandes, H. R.; Gaddam, A.; Rebelo, A.; Brazete, D.; Stan, G. E.; Ferreira, J. M. F. Bioactive Glasses and Glass-Ceramics for Healthcare Applications in Bone Regeneration and Tissue Engineering. *Materials* **2018**, *11* (12), 2530.

(21) Palumbo, F. S.; Federico, S.; Pitarresi, G.; Fiorica, C.; Giammona, G. Synthesis and Characterization of Redox-Sensitive Polyurethanes Based on L-Glutathione Oxidized and Poly(Ether Ester) Triblock Copolymers. *React. Funct. Polym.* **2021**, *166* (July), 104986.

(22) Shi, R.; Xue, J.; He, M.; Chen, D.; Zhang, L.; Tian, W. Structure, Physical Properties, Biocompatibility and in Vitro/Vivo Degradation Behavior of Anti-Infective Polycaprolactone-Based Electrospun Membranes for Guided Tissue/Bone Regeneration. *Polym. Degrad. Stab.* **2014**, *109*, 293–306.

(23) Bennour, S.; Louzri, F. Study of Swelling Properties and Thermal Behavior of Poly(N,N-Dimethylacrylamide- Co -Maleic Acid) Based Hydrogels. *Adv. Chem.* **2014**, *2014*, 1–10.

(24) Baskic, D.; Popovic, S.; Ristic, P.; Arsenijevic, N. Analysis of Cycloheximide-Induced Apoptosis in Human Leukocytes: Fluorescence Microscopy Using Annexin V/Propidium Iodide versus Acridin Orange/Ethidium Bromide. *Cell Biol. Int.* **2006**, *30* (11), 924–932.

- (25) Matos-Pérez, C. R.; Wilker, J. J. Ambivalent Adhesives: Combining Biomimetic Cross-Linking with Antiadhesive Oligo-(Ethylene Glycol). *Macromolecules* **2012**, *45* (16), 6634–6639.
- (26) Zhou, J.; Defante, A. P.; Lin, F.; Xu, Y.; Yu, J.; Gao, Y.; Childers, E.; Dhinojwala, A.; Becker, M. L. Adhesion Properties of Catechol-Based Biodegradable Amino Acid-Based Poly(Ester Urea) Copolymers Inspired from Mussel Proteins. *Biomacromolecules* **2015**, *16* (1), 266–274.
- (27) Xu, Z.; Chen, L.; Lu, L.; Du, R.; Ma, W.; Cai, Y.; An, X.; Wu, H.; Luo, Q.; Xu, Q.; Zhang, Q.; Jia, X. A Highly-Adhesive and Self-Healing Elastomer for Bio-Interfacial Electrode. *Adv. Funct. Mater.* **2021**, *31* (1), 2006432.
- (28) Than, Y. M.; Suriyarak, S.; Titapiwatanakun, V. Rheological Investigation of Hydroxypropyl Cellulose-Based Filaments for Material Extrusion 3D Printing. *Polymers* **2022**, *14* (6), 1108.
- (29) Mackay, M. E. The Importance of Rheological Behavior in the Additive Manufacturing Technique Material Extrusion. *J. Rheol.* **2018**, *62*, 1549–1561.
- (30) Aho, J.; Boetker, J. P.; Baldursdottir, S.; Rantanen, J. Rheology as a Tool for Evaluation of Melt Processability of Innovative Dosage Forms. *Int. J. Pharm.* **2015**, *494* (2), 623–642.
- (31) Nguyen, N. A.; Bowland, C. C.; Naskar, A. K. A General Method to Improve 3D-Printability and Inter-Layer Adhesion in Lignin-Based Composites. *Appl. Mater. Today* **2018**, *12*, 138–152.
- (32) Suwardie, H.; Wang, P.; Todd, D. B.; Panchal, V.; Yang, M.; Gogos, C. G. Rheological Study of the Mixture of Acetaminophen and Polyethylene Oxide for Hot-Melt Extrusion Application. *Eur. J. Pharm. Biopharm.* **2011**, *78* (3), 506–512.
- (33) Elbadawi, M.; Gustaffson, T.; Gaisford, S.; Basit, A. W. 3D Printing Tablets: Predicting Printability and Drug Dissolution from Rheological Data. *Int. J. Pharm.* **2020**, *590*, 119868.
- (34) Azad, M. A.; Olawuni, D.; Kimbell, G.; Badruddoza, A. Z. M.; Hossain, M. S.; Sultana, T. Polymers for Extrusion-Based 3D Printing of Pharmaceuticals: A Holistic Materials-Process Perspective. *Pharmaceutics* **2020**, *12* (2), 124.
- (35) Hufert, J.; Grebhardt, A.; Schneider, Y. Deformation Behavior of 3D Printed Auxetic Structures Of Thermoplastic Polymers: PLA, PBAT, and Blends. *Polymers* **2023**, *15* (2), 389.
- (36) Alsoufi, M. S.; Elsayed, A. E. How Surface Roughness Performance of Printed Parts Manufactured by Desktop FDM 3D Printer with PLA+ Is Influenced by Measuring Direction. *Am. J. Mech. Eng.* **2017**, *5* (5), 211–222.
- (37) Patti, A.; Acierno, S.; Cicala, G.; Acierno, D. Predicting the Printability of Poly(Lactide) Acid Filaments in Fused Deposition Modeling (FDM) Technology: Rheological Measurements and Experimental Evidence. *ChemEngineering* **2023**, *7* (1), 1.
- (38) Elbadawi, M. Polymeric Additive Manufacturing: The Necessity and Utility of Rheology. In *Polymer Rheology*; InTech, 2018.
- (39) Kollamaram, G.; Croker, D. M.; Walker, G. M.; Goyanes, A.; Basit, A. W.; Gaisford, S. Low Temperature Fused Deposition Modeling (FDM) 3D Printing of Thermolabile Drugs. *Int. J. Pharm.* **2018**, *545* (1–2), 144–152.